Neurotox Res (2017) 31:187–203
DOI 10.1007/s12640-016-9666-9

ORIGINAL ARTICLE

Developmental Injury to the Cerebellar Cortex Following Hydroxyurea Treatment in Early Postnatal Life: An Immunohistochemical and Electron Microscopic Study

Joaquín Martí[1] · Vanesa Molina[1] · M. C. Santa-Cruz[1] · José P. Hervás[1]

Received: 10 June 2016 / Revised: 17 August 2016 / Accepted: 30 August 2016 / Published online: 6 September 2016

Abstract Postnatal development of the cerebellar cortex was studied in rats administered with a single dose (2 mg/g) of the cytotoxic agent hydroxyurea (HU) on postnatal day (P) 9 and collected at appropriate times ranging from 6 h to 45 days. Quantification of several parameters such as the density of pyknotic, mitotic, BrdU-positive, and vimentin-stained cells revealed that HU compromises the survival of the external granular layer (EGL) cells. Moreover, vimentin immunocytochemistry revealed overexpression and thicker immunoreactive glial processes in HU-treated rats. On the other hand, we also show that HU leads to the activation of apoptotic cellular events, resulting in a substantial number of dying EGL cells, as revealed by TUNEL staining and at the electron microscope level. Additionally, we quantified several features of the cerebellar cortex of rats exposed to HU in early postnatal life and collected in adulthood. Data analysis indicated that the analyzed parameters were less pronounced in rats administered with this agent. Moreover, we observed several alterations in the cerebellar cortex cytoarchitecture of rats injected with HU. Anomalies included ectopic placement of Purkinje cells and abnormities in the dendritic arbor of these macroneurons. Ectopic granule cells were also found in the molecular layer. These findings provide a clue for investigating the mechanisms of HU-induced toxicity during the development of the central nervous system. Our results also suggest that it is essential to avoid underestimating the adverse effects of this hydroxylated analog of urea when administered during early postnatal life.

Keywords Postnatal · Hydroxyurea · Cerebellum · Ectopia · Purkinje cells · Granule cells

Introduction

The mammalian cerebellum is a foliated structure consisting of a central vermis and two bilateral hemispheres (Jacobs et al. 2014; Cerminara et al. 2015). This organ has a regular organization composed of the cerebellar cortex and an aggregate of neurons that constitutes the deep cerebellar nuclei (Sillitoe and Joyner 2007; Sultan and Glickstein 2007). Neuroembryological studies have indicated that the isthmic constriction, the neural tissue at the metencephalic–mesencephalic junction, directs the formation of the cerebellar territory (Martínez et al. 2013). It is accepted that the organizing activity of the isthmic tissue is mediated by the fibroblast growth factor 8 (Nakamura et al. 2008; Suzuki-Hirano et al. 2010). The establishment of the cerebellar territory is followed by the formation of two germinative compartments with distinct developmental potentialities, the ventricular zone and the rhombic lip (Dastjerdi et al. 2012; Butts et al. 2014; Marzban et al. 2015). The first of these originates GABAergic neurons; the second produces glutamatergic cells (Wullimann et al. 2011; Leto et al. 2012; Martínez et al. 2013).

Granule cell (GC) precursors emerge from the rhombic lip and migrate tangentially over the pia mater to form the external granular layer (EGL), a transient proliferative structure (Altman and Bayer 1997). During early postnatal development, neuroblasts in the EGL proliferate and

✉ Joaquín Martí
joaquim.marti.clua@uab.es

[1] Unidad de Citología e Histología, Facultad de Biociencias, Universidad Autónoma de Barcelona, Bellaterra, 08193 Barcelona, Spain

postmitotic GCs reach the inner part of this germinal matrix, starting to differentiate. These microneurons then migrate along the processes of Bergman glia cells and populate the internal granular layer (IGL) (Komuro et al. 2001; Chedotal 2010; Xu et al. 2013). During the same period as the proliferation, migration, and differentiation of GCs, the Purkinje cell (PC) dendrites extend and branch, eventually developing into their sophisticated adult dendritic tree (Carletti and Rossi 2008; Tanaka 2015).

Hydroxyurea (HU) is a drug used for the treatment of various types of cancer (Saban and Bujak 2009), myeloproliferative diseases, and sickle-cell anemia (Navarra and Preziosi 1999; Ware et al. 2011). This chemical compound is also used for the management of dermatological diseases (Lebwohl et al. 2004) and HIV infection (Zala et al. 2000). HU inhibits DNA synthesis of proliferating cells through ribonucleotide reductase inactivation (Shao et al. 2006; Newton 2007; Saban and Bujak 2009).

There are many reports of HU-related teratogenic effects. When administered to pregnant dams, it induces—in the offsprings—alterations in the craniofacial tissues (Schlisser and Hales 2013) and growth retardation (Woo et al. 2004). HU also produces microcephaly (Woo et al. 2004), apoptosis in neuroepithelial cells (Woo et al. 2003, 2006), and systematic differences in the neurogenetic timetables and neurogenetic gradients of PCs and deep cerebellar nuclei neurons (Martí et al. 2016).

Despite data concerning the deleterious effects of HU on embryonic life, few studies (to our knowledge) have analyzed the effect of this drug on the development of the central nervous system by focusing on postnatal life. We have some evidence showing that HU exposure in the early postnatal life produces cell depletion in the cerebellar EGL and ectopic location of GCs (Ebels et al. 1975; Koppel et al. 1983). Despite this evidence, the influence of this hydroxylated derivate of urea on the postnatal development of rat cerebellum has not been completely elucidated.

In light of the above, we began a set of experiments in our laboratory. The major goal of this article is to analyze, at postnatal day (P) 9, the effect of HU treatment on the development of rat cerebellum. This age was not selected at random but, instead, selected because in normal rats, it is about P9 when the EGL reaches its greatest thickness, PCs are dispersed into a monolayer, and a clearly delineated IGL is seen (Altman and Bayer 1997). Choice of cerebellum was supported by the evidence that this region of the central nervous system is one of the most experimentally tractable systems in the brain (Martínez et al. 2013; Butts et al. 2014). The cerebellum presents a stereotypical laminar organization. It is composed of only a few cell types, all organized in a precise fashion in distinct morphological layers (Marzban et al. 2015). Additionally, the cerebellum is highly vulnerable to intoxication (Manto 2012). The study of the HU treatment on the development rat cerebellum can serve as a model to analyze and interpret the toxic effects of this organic compound in the rest of the brain, and indeed also outside of the nervous system.

Specifically, the following aspects were addressed: (I) we characterized the effect of HU administration on the EGL cells. This was carried out by quantifying the density of pyknotic, mitotic, and 5-bromo-2′-deoxyuridine (BrdU) reactive cells after a single dose of the cytotoxic agent HU. The expression of the cytoskeletal protein vimentin was also studied. (II) Neuroapoptosis has been reported during the normal development of the cerebellum (Contestabile 2002; Lossi and Gambino 2008; Jankowski et al. 2009). Cerebellar neurons apoptosis is also induced by toxic factors, including platinum compounds (Pisu et al. 2004; Bernocchi et al. 2011; Cerri et al. 2011), glucocorticoids (Cabrera et al. 2014), ethanol (Oliveira et al. 2014), and heroin (Pu et al. 2015). Previous data have indicated that HU induces apoptosis in the telencephalon of fetal rats (Woo et al. 2003, 2006). To characterize the type of cell death in EGL neuroblasts induced by HU treatment, we used terminal deoxynucleotidyl transferase dUTP nick-end labeling (TUNEL) and transmission electron microscopy for diagnosing apoptotic degeneration. (III) In rats exposed to HU in early postnatal life and collected in adulthood, we quantified several parameters of the cerebellar cortex. Features were as follows: (I) length of the cerebellar cortex, (II) area of the ML, (III) density of PCs, (IV) area of the IGL, (V) GCs density, and (VI) percentage of BrdU-stained GCs. In addition, we examined the spatial location of PCs and GCs. The morphology of the PC dendritic tree was also studied.

Materials and Methods

Animals and Treatments

All experiments in this study were carried out in accordance with the requirements of the Committee for Institutional Animal Care and Use in the Universitat Autònoma de Barcelona (UAB). The number of animals was kept to a minimum, and all efforts were made to minimize their suffering. Pregnant Sprague–Dawley OFA rats were obtained from the animal production facility at the UAB. Postnatal offspring was a result of timed pregnancies. On P1, the number of pups and percentage of males and females in each litter were counted. Thereafter, the number in each litter was culled to 10, and pups were cross-fostered, so that one mother raised 5 saline pups and 5 HU-exposed pups. Whenever possible, the same number of male and female pups was kept in each litter.

Based on published studies of developmental toxicity of HU (Ebels et al. 1975; Koppel et al.1983), the dose of 2 mg/g b.w was chosen. A total of 90 pups of either sex were injected intraperitoneally, at P9, with a single injection of saline (0.9 % NaCl) (45 rats) or HU (Sigma, St. Louis, MO, USA) (2 mg/g b.w) (45 rats). At regular intervals from 6 to 24 h and on 48 and 72 h after saline or HU exposure (10 rats per stage, 5 were injected with saline and 5 with HU), animals were killed. Before sacrifice, rats from both experimental groups (saline and HU) were administered intraperitoneally with a single dose of BrdU (Sigma, St. Louis, MO, USA) (50 mg/kg b.w) dissolved in sterile saline solution with 0.007 N sodium hydroxide. Rats were allowed to survive for 2 h after delivering this marker. Schedules and the number of animals per experimental group are listed in Table 1.

In the second set of experiments, 10 rats were administered intraperitoneally, at P9, with a single injection of saline (5 animals) or HU (2 mg/g b.w) (5 animals). After this treatment, rats from both experimental groups (saline and HU) were administered with BrdU (50 mg/kg b.w; intraperitoneal) at P12. Animals were observed daily after HU exposure, and their body weights recorded every three days until they were sacrificed at P45.

Embryonic day (E)1 was deemed to be the morning after mating; date of birth was P0. All rat pups were weaned at P21 by separating them from their mothers and housing them in individual cages. During the experimental procedures, animals were maintained in a quiet room with controlled conditions (a 12-h light/dark cycle, 22 ± 2 °C, food and water were provided ad libitum).

The following features were recorded to determine the effect of postnatal exposure to HU: body weight gain, body weight, and percentage of rats survived until P45.

Perfusion and Histology

At appropriate times, the rats were anesthetized with ketamine–xylazine mixture (90:10 mg/ml; 1 ml/kg, intraperitoneal) and transcardially perfused with 4 % paraformaldehyde in 0.1 M phosphate buffer, pH 7.3. The brains were immediately removed, dissected, and post-fixed in the same fixative medium at 4 °C for 24 h. These were embedded in paraffin following the regular procedures of our laboratory. Cerebella were serially cut in the sagittal plane at 10 μm. Only those sections representative of the medial point of the vermis were used in the study. This region is characterized by the limited presence of fastigial neurons. No sections containing cerebellar hemispheres were studied. One in every five sections was placed on poly-(L-lysine)-coated slides for subsequent processing. Each slide had one complete section of the cerebellum.

Table 1 Schedules of saline, hydroxyurea, and bromodeoxyuridine administrations

Treatment	Time (h)								
P9	6	9	12	15	18	21	24	48	72
Saline[5]	I; S								
Saline[5]		I; S							
Saline[5]			I; S						
Saline[5]				I; S					
Saline[5]					I; S				
Saline[5]						I; S			
Saline[5]							I; S		
Saline[5]								I; S	
Saline[5]									I; S
HU (2 mg/g)[5]	I; S								
HU (2 mg/g)[5]		I; S							
HU (2 mg/g)[5]			I; S						
HU (2 mg/g)[5]				I; S					
HU (2 mg/g)[5]					I; S				
HU (2 mg/g)[5]						I; S			
HU (2 mg/g)[5]							I; S		
HU (2 mg/g)[5]								I; S	
HU (2 mg/g)[5]									I; S

P postnatal day, *I* a single injection of bromodeoxyuridine (50 mg/kg), *S* sacrifice after bromodeoxyuridine exposure (1 h), *HU* hydroxyurea. In brackets is the number of rats used

Feulgen Method

Feulgen staining was performed according to previously published procedures (Hervás et al. 2002; Martí et al. 2015). Sections were deparaffinized in xylene and rehydrated through a series of graded ethanols. Partial denaturation of DNA was carried out by 3 N HCl at 40 °C for 15 min. Hydrolysis was halted by two washes in distilled water at RT and then treated 1 h in darkness with Schiff's reagent (prepared from basic fuchsin; Fluka Chemie, Buchs, Switzerland) at RT. After washing in a fresh sulphurous acid solution, the stained sections were rinsed in distilled water, dehydrated, and cover-slipped.

Immunocytochemistry

Immunoperoxidase staining for BrdU was performed according to previous procedures (Hervás et al. 2002; Martí et al. 2015). Partial denaturation of DNA was carried out by 3 N HCl for 30 min at 40 °C in previously deparaffinized sections. Hydrolysis was halted by two washes in distilled water, the first at 4 °C and the second at RT. Endogenous peroxidase activity was blocked as mentioned above. After this, slides were washed in 0.5 % Triton X-100 in PBS, and incubated with the primary antibody (Dako, clone BU20a, Code No, M0744). This was diluted 1:150 in PBS supplemented with 1 % bovine serum albumin (BSA, Boheringer Mannheim, Germany).

For calbindin D-28 k immunohistochemistry, deparaffinized sections were treated for 10 min with 3 % H_2O_2 in methanol. Nonbinding sites were blocked using 5 % bovine serum albumin in PBS containing 0.1 % Tween-20 and 5 % normal goat serum for 1 h at room temperature. Following this, the slides were incubated at 4 °C with monoclonal mouse anti-calbindin D-28 k (1:1000, Swant, Lot No: 07F, Code No: 300) for 72 h.

Following incubation in primary antibodies, sections were incubated for 1 h at room temperature with an anti-mouse Immunoglobulin, Biotin Conjugated, produced in goat (Sigma) 1:20, and then exposed to ExtrAvidin–peroxidase (Sigma) 1:20 for 30 min. Peroxidase activity was developed by 3,3′-diaminobenzidine–H_2O_2 (Sigma) for 5 min, and were finally rinsed in distilled water and counterstained with haematoxylin.

Vimentin immunohistochemistry was performed in deparaffinized sections. These were soaked in 3 % H_2O_2 in methanol for 10 min and incubated with TBS-EDTA containing Tween-20 for 25 min in a water bath at 90 °C. The slides were then allowed to cool to room temperature for at least 30 min. Nonbinding sites were blocked using 0.5 % bovine serum albumin in TBS containing 5 % of fetal calf serum and Triton X-100. Subsequently, the slides were incubated overnight at 4 °C with a mouse monoclonal anti-vimentin (1:50; Dako, M0725). After this, sections were rinsed with TBS containing Tween-20 and incubated at room temperature for 30 min with a biotin-conjugated goat anti-mouse IgG antibody (Sigma) 1:50 for 30 min and then exposed to ExtrAvidin–peroxidase (Sigma) 1:50 for 30 min. Peroxidase activity was developed by 3,3′-diaminobenzidine-H_2O_2 (DAB, Sigma) for 5 min, and were then rinsed in distilled water.

In all protocols, control sections were prepared replacing the primary antibody by PBS; they routinely showed no immunolabeling.

TUNEL Staining

Each TUNEL or immunohistochemical reaction was simultaneously performed in all rats within a given experiment to maximize the reliability of comparison across groups. TUNEL staining was done with an in situ cell death detection kit (POD Roche Diagnostics, cat 11684817910). In brief, after removing paraffin, sections were incubated with proteinase K, nuclease free (20 µg/ml in 10 mM Tris–HCl, pH 7.5) for 30 min at room temperature. They were then cleaned with PBS and incubated for 10 min with 3 % H_2O_2 in methanol. Slices were soaked in the TUNEL reaction mixture for 60 min at 37 °C and then cleaned with PBS. Subsequently, sections were incubated with converted POD for 30 min at 37 °C. After further rinsing in PBS, the peroxidase coloring reaction was developed by 3,3′-diaminobenzidine–H_2O_2 for 5 min, and were then rinsed in distilled water and counterstained with haematoxylin. For positive control of TUNEL labeling, histological sections were incubated with DNase (5 µg/ml) for 10 min at 37 °C to induce DNA strand breaks.

Transmission Electron Microscopy

Animals were anesthetized with ketamine–xylazine mixture (90:10 mg/ml; 1 ml/kg, intraperitoneal) and transcardially perfused with 2 % glutaraldehyde, 2 % paraformaldehyde in 0.1 M cacodylate buffer, pH 7.2. Brains were removed, dissected, and fixed in fresh fixative overnight at 4 °C. Tissues cubes ($\sim$1 mm^3) were rinsed in PBS, postfixed in 1 % OsO_4 for 2 h, dehydrated in a graded ethanol series, infiltrated with propylene oxide, and embedded in Epon. Ultrathin sections (60 nm) were generated by an ultramicrotome (Leica AG, Reichert ultracut S) and were viewed with a transmission electron microscope (JEM-1400). Digital images were acquired with a CCD GATAN 794 MSC 600HP digital camera system and analyzed using Adobe Photoshop software.

Quantitative Analyses

Counts of pyknotic, mitotic, BrdU-labeled, and vimentin-positive cells in the EGL were carried out, at 100X oil immersion objective, in the pertinent sections, by visual scanning of the cerebellar cortex throughout the entire anteroposterior profile. Criteria for scoring pyknotic cells included both morphological and staining properties (condensed, fragmented, and densely stained nuclei) in Feulgen-stained sections. Mitotic cells were identified by their typical characteristics with the reaction of Schiff. EGL cells were counted on the basis of several assumptions such as size and distinctive stain properties. Small darkly stained and densely packed cells, most round-like in shape, were considered as EGL cells. The BrdU-stained GCs can be recognized by the presence of a bright brown pigment over their nuclei. Vimentin-immunoreactive Bergmann glial cells were defined as those that have a brown reaction product in both the cell body and glial process. The immunostaining intensity was strong enough to allow a confident distinction of labeled cells. No background was observed.

In rats collected at P45, the following features of the cerebellar morphology were quantified: (I) length of the cerebellar cortex, (II) area of the ML, (III) density of PCs, (IV) area of the IGL, (V) GCs density, and (VI) percentage of BrdU-stained GCs. Each parameter was determined in three sections containing the entire cerebellum of every experimental rat. Data from each section were combined to obtain a mean for each cerebellar feature per rat. All the cerebellar parameters quantified in the current paper are typical for cerebellar morphology (Bauer-Moffett and Altman 1977; Smeyne and Goldowitz 1989; Martí et al. 2015, 2016). The level used for quantitative analysis is that indicated in the Paxinos and Watson atlas (Paxinos and Watson 1998): from figure 79 (lateral −0.10 mm) to figure 79a (lateral 0.18 mm).

Measurements were carried out as previously reported (Martí et al. 2013; 2015). Under identical lighting conditions, images were captured by a CCD-IRIS color video camera (Sony, Japan) coupled to a Zeiss Axiophot microscope and digitalized. Morphometric analysis was performed with the Visilog 5 software (Noesis, France). Analysis was as follows: first, calibration to convert pixel units to metric units. Subsequently, the length of the cerebellar cortex and the contour of the EGL and the ML were manually delimited to obtain initial binary images. These images were submitted to the indicated software so as to accurately measure the length of the cerebellar cortex and the area of the EGL and ML in every analyzed region.

Qualitative Analyses

Light microscopic observations were made with a Zeiss Axiophot microscope using a wide set of objectives ranging from 2.5 to 100×. Observations were focused at the foliar crowns from the anterior lobe (lobules I to V), the central lobe (VI to VIII), the posterior lobe (IX), and the inferior lobe (X). The depth of the prima and secunda was also studied. The limits between foliar crowns and fissures were set as reported (Martí et al. 2007). This consisted of digitally capturing images from wild-type and homozygous *weaver* mice cerebella with a CCD-IRIS color video camera (Sony, Japan) coupled to a Zeiss Axiophot microscope equipped with a 40× oil immersion objective. By means of software (Visilog 5, Noesis, France), two outlines were drawn. The first of these delimited the cerebellar cortex surface, while the second was performed by tracing the angle bisector in a given fissure corner. The points of intersection on both sides represented the two outer limits of the fissure. The space included between two successive fissures was considered as a foliar crown.

Data Analysis

The statistical significance of the results was evaluated with the Student's *t* test or Mann–Whitney *U* test. When more than two means were simultaneously compared, the one-way ANOVA followed by individual comparison of means with the Student–Newman–Keuls (SNK) test were used.

Photographic Material

Photographic material was captured by a CCD-IRIS color video camera (Sony, Japan), coupled to a Zeiss Axiophot microscope. The digitized images were processed in the Adobe Photoshop software.

Results

Experiment 1

During the early postnatal life, the EGL gives rise to the most abundant cerebellar neuronal population, the GCs (Chedotal 2010). This region contains proliferative neuroblasts, the precursors of GCs (Altman and Bayer 1997). Cellular demise may be induced by toxic agents, which disrupt the generative behavior of GCs precursors. This experiment was carried out to study the effect of HU treatment, an cytostatic drug that inhibits DNA synthesis of proliferating cells (Saban and Bujak 2009), on EGL cells and to examine the ability of this germinal matrix to

resume proliferative activity. This was undertaken by quantifying the density of pyknotic, mitotic, and BrdU-reactive cells per millimeter of length of the cerebellar cortex. The expression of the cytoskeletal protein vimentin was also analyzed. Data of the measured parameters in rats collected from 6 to 72 h after HU exposure, in addition to the statistical analysis of the former parameters, are depicted in Fig. 1a–d. Results indicated that the density of pyknotic cells increased from 6 to 24 h after HU exposure. After 24 h, the values declined. No differences were seen in animals collected 72 h after drug exposure. On the other hand, neither mitotic nor BrdU-stained cells were seen until 21 h after drug administration. After such time, the density of both parameters increased until 72 h after treatment, but they did not achieve saline values. When the density of vimentin-positive cell bodies was considered, values decreased in each studied timepoint. Moreover, from 24 to 72 h, vimentin immunocytochemistry revealed overexpression and thicker immunoreactive glial processes in HU-treated rats (Fig. 1e, f). Two facts emerge from these data: (I) the administration of HU induces deleterious effects on the EGL, (II) mitotic and BrdU-immunoreactive cells were seen 21 h after drug injury, suggesting that the EGL recovered proliferative activity.

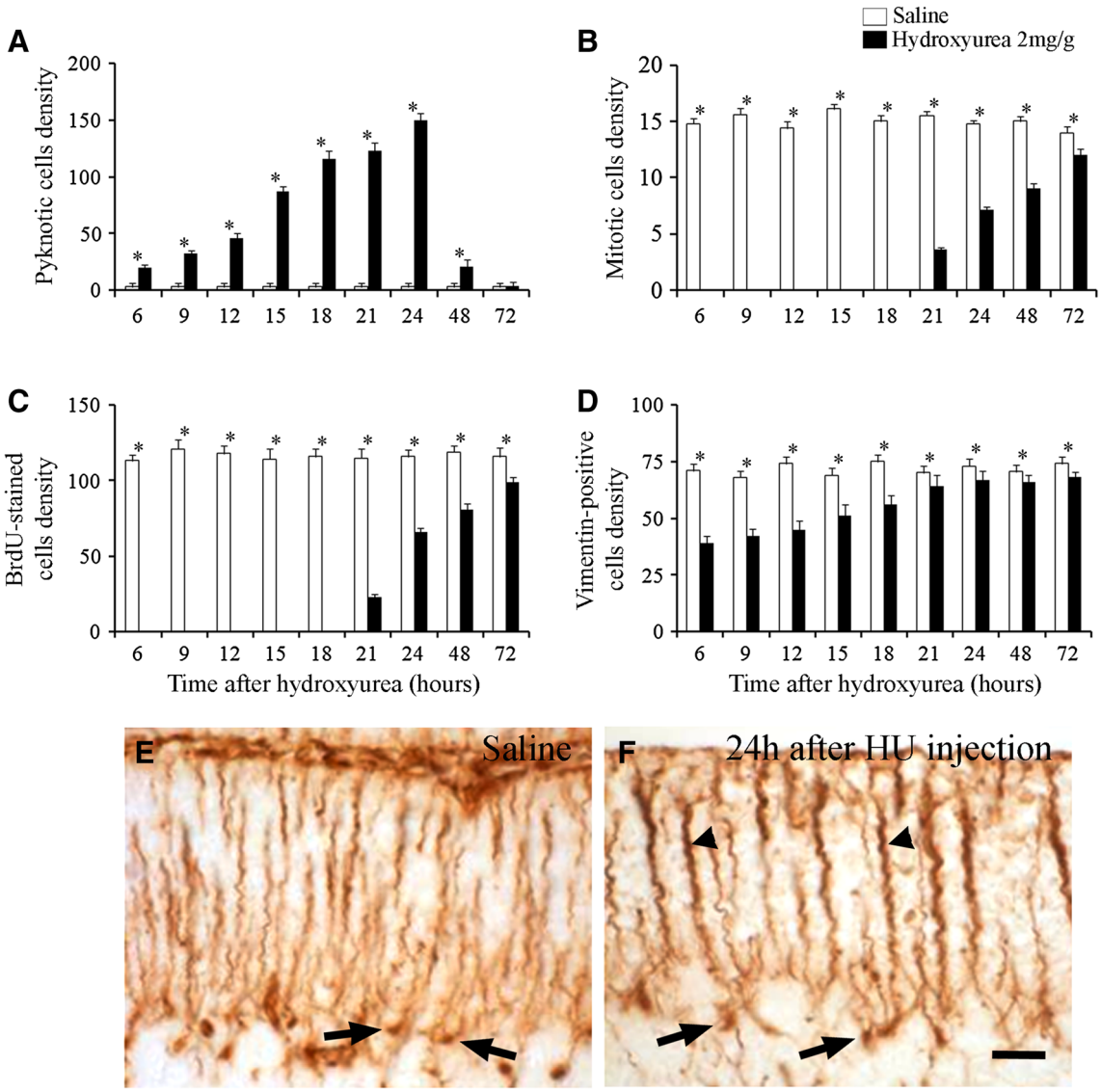

Fig. 1 Mean ± SEM for pyknotic (**a**), mitotic (**b**), BrdU-positive (**c**), and vimentin-positive cells. (**d**) Density is presented in rats injected with saline (white columns) or hydroxyurea (*black columns*) and survival several hours after treatment. *Indicates statistical significance, $p < 0.05$. Distribution of vimentin in the cerebellar cortex of a saline (**e**) and a HU-injected rat (**f**). In the saline (**e**), vimentin-positive Bergmann fibers are arranged in the typical palisade configuration. Immunoreactivity is also observed in the small cell bodies of this glial type (*arrows*). After HU exposure (24 h), Bergmann fiber appears thicker and intensely immunostained (*arrow heads*). *Scale bar* 20 μm

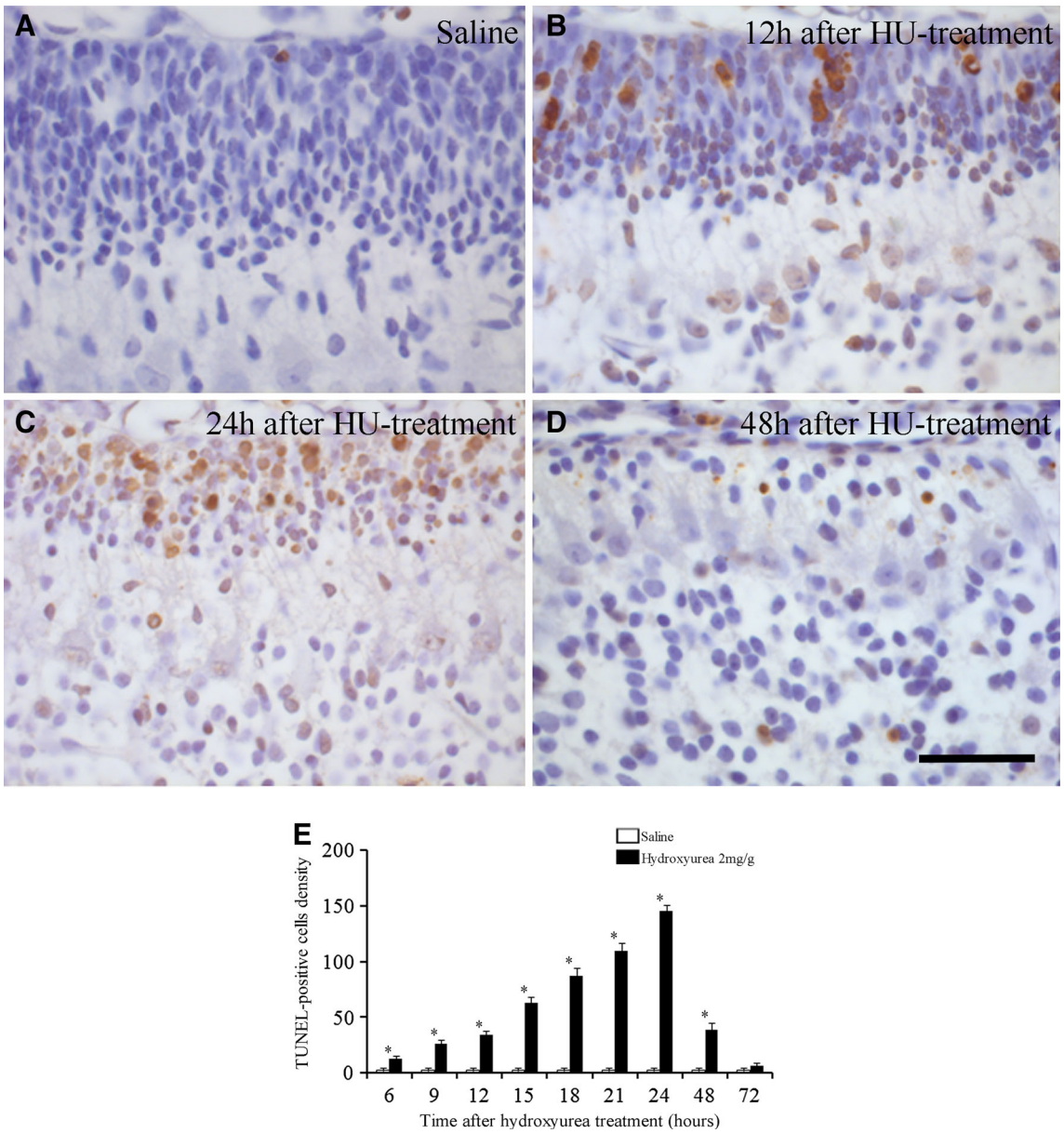

Fig. 2 Microscopic detection of TUNEL-positive cells in rats treated with saline or hydroxyurea at postnatal day 9 and collected at appropriate times. TUNEL-positive cells are those presenting a brown reaction product in their nuclei. **a** A few scattered TUNEL-positive cells are observed in the external granular layer of saline rats. **b** 12 h after HU injection, numerous TUNEL-positive cells were observed in this germinal matrix. **c** Massive cell death is found following 24 h of treatment. **d** The number of TUNEL-stained cells decreased after 48 h of treatment. Note that HU administration is associated with a considerable reduction in the external granular layer thickness. *Scale bar* 30 µm. **e** Mean values for TUNEL-positive cells density ± SEM and statistical data analysis are presented in rats injected with saline or hydroxyurea and survival several hours after treatment. *Indicates statistical significance, $p < 0.05$

Experiment 2

Previous results have revealed that HU produces apoptosis in the mouse fetal telencephalon (Woo et al. 2003, 2006). In this study, we have chosen to treat rats with HU. As a consequence, apoptotic cellular events may be activated, resulting in a substantial number of dying cells. The aim of our research was to characterize, in the early postnatal life, the type of cell death of EGL cells induced by HU exposure. We used TUNEL reaction and transmission electron microscopy for diagnosing apoptotic degeneration. Figure 2a–d epitomizes the variation in the density of TUNEL-positive cells in the EGL of rats exposed to HU at P9 and surviving until 72 h after drug administration. Numbers of TUNEL-reactive cells as well as the statistical analysis of the former parameter are depicted in Fig. 2e. Results indicated that the density of TUNEL-reactive cells increased after 6 h and peaked at 24 h, after that, the values

declined. No differences were seen in animals collected 72 h after drug exposure.

Apoptosis can be defined by a series of stereotyped ultrastructural features according to a well-defined sequence of events (Elmore 2007). To our knowledge, there are no studies providing detailed ultrastructural features for recognizing cellular apoptosis in the EGL of rats exposed to HU. In the absence of such criteria, the description pertaining to the normal rat forebrain and cerebellum Dikranian et al. (2001), Lossi and Merighi (2003), and Lossi and Gambino (2008) has served as a reference standard. Current electron microscopic examination revealed that, in saline-administered animals, the EGL cells were of a normal structure. Briefly, they were closely packed with nuclei, occupying almost all the cell body, exhibited clumps of condensed chromatin and heterochromatin associated with the nuclear membrane, and dispersed through the nucleoplasm (Fig. 3a). In HU-treated rats, apoptotic neuroblasts were found in the EGL. Our observations also indicated that at all the time points studied (from 6 to 72 h after HU exposure), different stages of apoptosis were observed (Fig. 3b–f). We describe a sequence of events, which are similar to those that characterize apoptotic neurodegeneration. The earliest morphological alterations were the condensation of chromatin, and its segregation at the nuclear periphery. Chromatin compaction appeared associated with convolution of nuclear envelope, giving a star-like nuclear appearance (Fig. 3b). At the cytoplasmic level, apoptotic cells exhibited a high density of ribosomes, which seem to be in a monomeric state (Fig. 3c). These early changes were followed in the mid-apoptotic stage by nuclear fragmentation. Fragments were apparently devoid of membranes (Fig. 3d). In parallel with nuclear changes, the plasma membrane was still intact but the organelles were packed, most likely as a consequence of cytosol loss, and the cisternal spaces of the endoplasmatic reticulum were dilated (Fig. 3d). In the late stages, apoptotic cells exhibited several nuclear fragments and membrane blebs (Fig. 3e). Numerous clusters of apoptotic bodies, which exhibited acute cytoplasmic degradation and fragmentation, were also visualized (Fig. 3f).

To summarize, our current observations suggest that the HU administration during the early postnatal life activates apoptotic cellular events, resulting in a substantial number of dying cells.

Experiment 3

This experiment was performed to determine whether postnatal administration of HU induces body weight

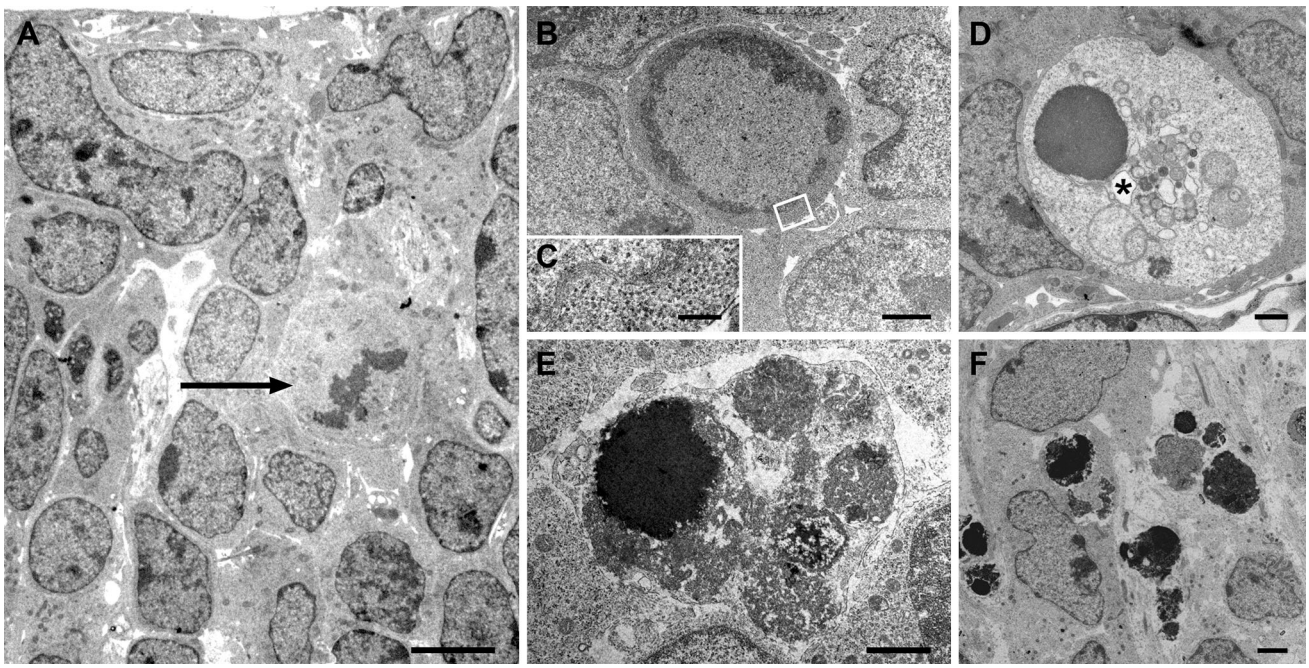

Fig. 3 Electron micrographs of healthy (**a**) and apoptotic neuroblasts in the external granular layer of rats administered with hydroxyurea and collected 24 h following drug treatment (**b–f**). Panel B shows an early apoptotic cell. Note the compact chromatin at the nuclear periphery. The area indicated by the *rectangle* is shown at higher magnification in (**c**). The latter illustrates, in the cytoplasm, the massive presence of ribosomes, which seem to be in a monomeric state. The mid-apoptotic stage (**d**) is distinguished by nuclear fragmentation. At the cytoplasmic level, the organelles are packed, and the cisternal spaces of the endoplasmatic reticulum are dilated (*asterisk*). **e**, **f** display late-apoptotic stage. Note that dying cells present nuclear fragments and membrane blebs (**e**). Typical clusters of apoptotic bodies can be seen exhibiting round and very electron-dense nuclear fragments. The membranes and organelles are destroyed (**f**). *Arrow* in **a** shows a mitotic figure. *Scale bar* in **a** 5 μm, in **b**, **d–f** 1 μm. **c** 200 nm

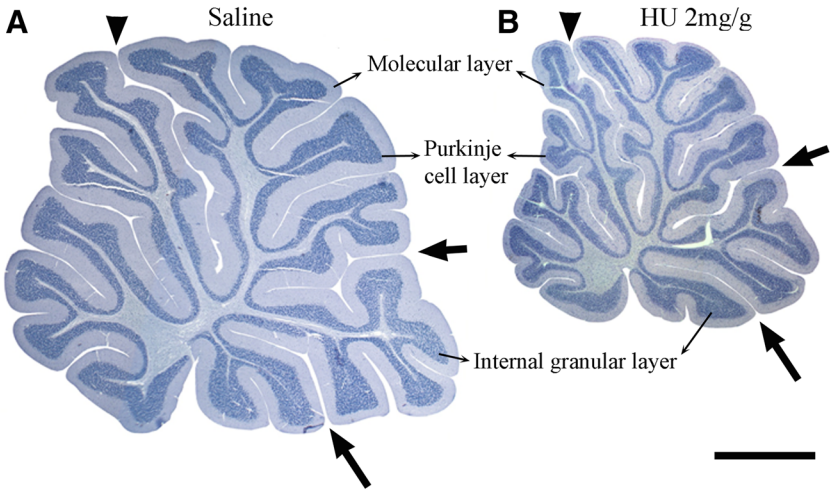

Fig. 4 Composite low-power photomicrographs of two midsagittal sections through rat cerebella collected at P45. The difference in cerebellar size between saline (**a**) and HU-treated rats (**b**) is evident. In both experimental groups, the vermis is divided along the anterior–posterior axis into four lobes: the anterior ranges from the rostral pole of the cerebellar cortex to the fissure prima (*arrowhead*), the central lobe between the fissura prima and the fissura secunda (*short arrow*), the posterior lobe between the secunda and the posterolateralis (*long arrow*), and the inferior lobe. *Scale bar* 1 mm

alterations or produces mortality. To this end, several features were recorded: (I) body weight gain, (II) body weight, and (III) percentage of rats survived until P45. In addition, we determine whether, and how, the administration of HU in the early postnatal life alters the development of the cerebellar cortex in rats sacrificed in the adulthood (P45). To this end, two approaches were undertaken: (1) Quantification of several features of the cerebellar cortex. These parameters were (I) length of the cerebellar cortex, (II) area of the ML, (III) density of PCs, (IV) area of the IGL, (V) GCs density, and (VI) density of BrdU-stained GCs. (2) To test whether HU exposure modifies the spatial location of PCs and GCs, and to examine the morphology of the PC dendritic tree.

Current results indicate that postnatal administration of HU modified neither body weight gain nor body weight. No mortality of any HU-injected rats was observed throughout the experimental period.

Sagittal sections from saline and HU-treated rats illustrating the lobular organization of the cerebellar cortex are shown in Fig. 4. In both experimental groups, cardinal fissures determining the limits among the four lobes of cerebellar cortex (prima, secunda, and posterolateralis) were present and were distinguishable. Figure 5 shows the BrdU-labeled GCs in saline and HU-treated rats. Data of the measured parameters in addition to the statistical analysis of the former parameters are depicted in Table 2. Significant effects were found in relation to saline, the HU condition always resulting in a decrease of quantified values.

Our study reveals that, in saline rats, the cerebellar cortex exhibited its typical layering. However, when the observations were focused on the HU-treated group, we detected anomalies in the cerebellar cytoarchitectonics. These included ectopic placement of PCs and abnormalities in their morphology. Ectopic GCs were also observed. Alterations were similar in all the HU-injected rats. They were not present in the saline group.

Sections immunostained for calbindin D-28 k revealed that, in animals injected with saline at P9 and surviving until P45, PCs were aligned in a monolayer and presented normal shapes. However, in the group receiving a single dose of 2 mg/g of HU, these macroneurons were piled 2–3 cell-thick (Fig. 6), and had the following morphological abnormalities in the dendrite tree (Fig. 7a–h): (I) in many neurons, each dendrite stem is bifurcated in a T-shape below groups of ectopic GCs; secondary dendrites apparently do not invade the upper ML (Fig. 7b, c), (II) in the same PCs, long-stem dendrites are deflected near ectopic GCs and seem to run parallel to the IGL surface, or else primary dendrite becomes obliquely derived from the vertical orientation (Fig. 7d–f), (III) the stem dendrite firstly ascends throughout the ML, but turns back below the ectopic GCs and then bifurcates in the proximity of PC somata (Fig. 7g), and (IV) the main dendrite is directed toward the IGL (Fig. 7h).

When GCs from rats administered with saline were considered, these microneurons were located in the IGL, and no ectopic location was seen. However, in rats exposed to HU, several GCs were arrested in the ML where they formed an ectopic zone. The position of the ectopic GCs presented four patterns (Fig. 8): (I) small clusters of cells located near the cerebellar surface. These were observed in the lobules I and X as well as in the deep prima and secunda fissures. (II) Alignment in a monolayer just

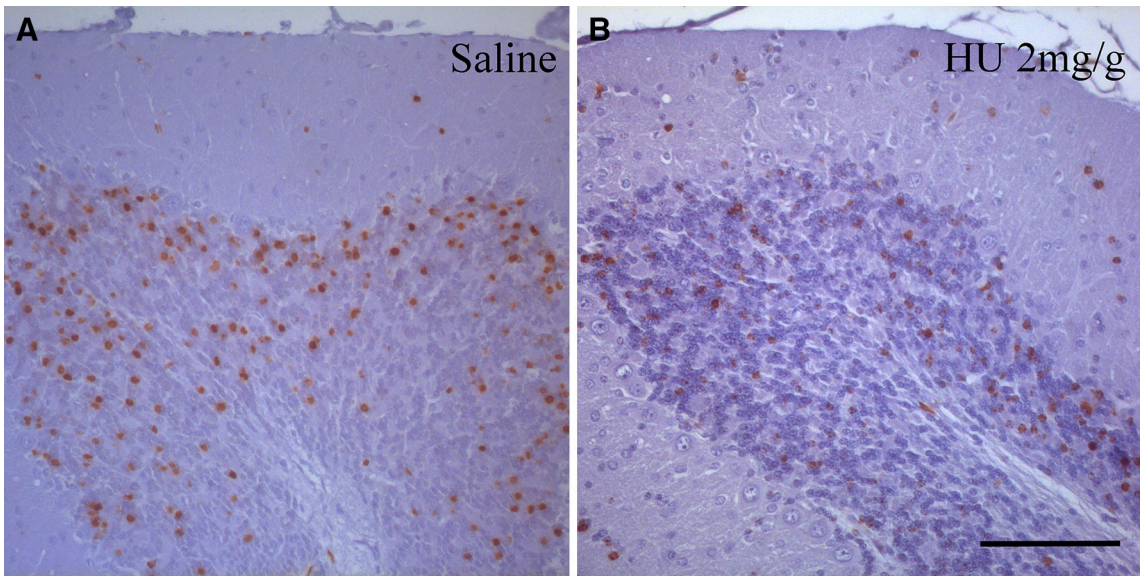

Fig. 5 Photomicrographs of BrdU-labeled granule cells from rats injected with saline (**a**) or hydroxyurea (**b**) at postnatal day 9 and surviving to postnatal day 45. BrdU-positive cells are those presenting a brown reaction product in their nuclei. Note that the HU administration is associated with a considerable reduction in the number of tagged granule cells. *Scale bar* 50 μm

Table 2 Mean values for several features in the region of the vermis and statistical analysis of the quantified parameters in rats injected with saline or hydroxyurea at early postnatal life and collected at postnatal day 45

Drug	Cortical length (mm)	Area ML (μm^2)	PCs density	Area IGL (mm^2)	GCs density	BrdU-labeled GCs/section
Saline	53.9 ± 1.5^a	9.4 ± 0.6^a	103.6 ± 3.8^a	2.5 ± 0.08^a	3109.6 ± 28.1^a	17.3 ± 1.2^a
HU (2 mg/g)	43.3 ± 1.2^b (80.3 %)	7.1 ± 0.5^b (75.5 %)	81.8 ± 3.4^b (79.0 %)	1.83 ± 0.04^b (73.2 %)	2371.8 ± 26.2^b (76.3 %)	8.9 ± 1.1^b (51.4 %)

Mean ± SEM are presented. *HU* hydroxyurea, *ML* molecular layer, *IGL* internal granular layer, *PCs* Purkinje cells, *GCs* granule cells. PCs and GCs density refer to the ratio neuron number respect to length of the cerebellar cortex. Numbers in parenthesis show percentages in relation to saline. *Indicates statistical significance $P < 0.05$ (*t* test or *U* test)

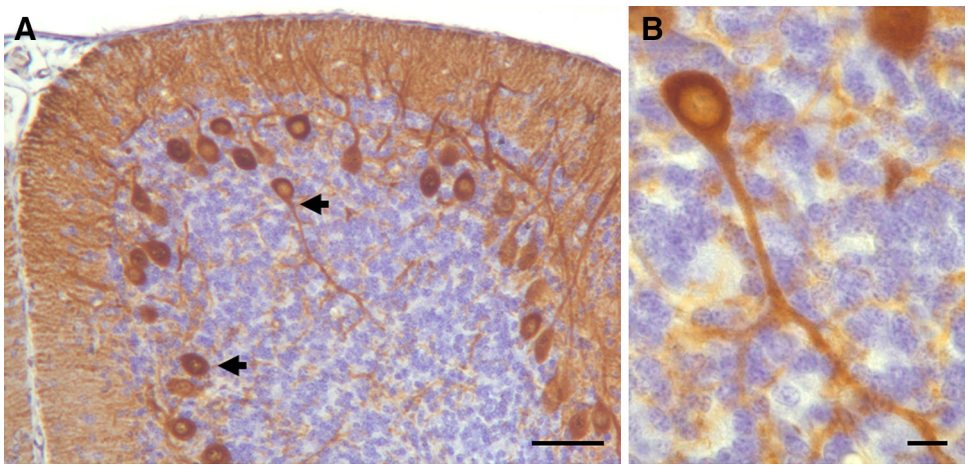

Fig. 6 Purkinje cell ectopia in HU-treated rats. **a** Calbindin-positive Purkinje cells (*arrows*) can be seen within the granular layer of the cerebellar cortex. **b** Higher magnification picture of an ectopic Purkinje cell shown in **a**. Note that the soma and dendritic tree are oriented to the depth of the granular layer. Micrographs correspond to the central lobe. *Scale bar* 50 μm (**a**), 10 μm (**b**)

beneath the pia mater. These were seen in the lobules II and III. (III) Imprecise aggregation in a thin strip oriented parallel to the pial surface. This band is usually found in the upper ML. These were found in the lobules IV, V, and IX. (IV) Occupation in the middle-to-lower part of the ML (lobules VI to VIII) and parallel to the pial surface. Patterns

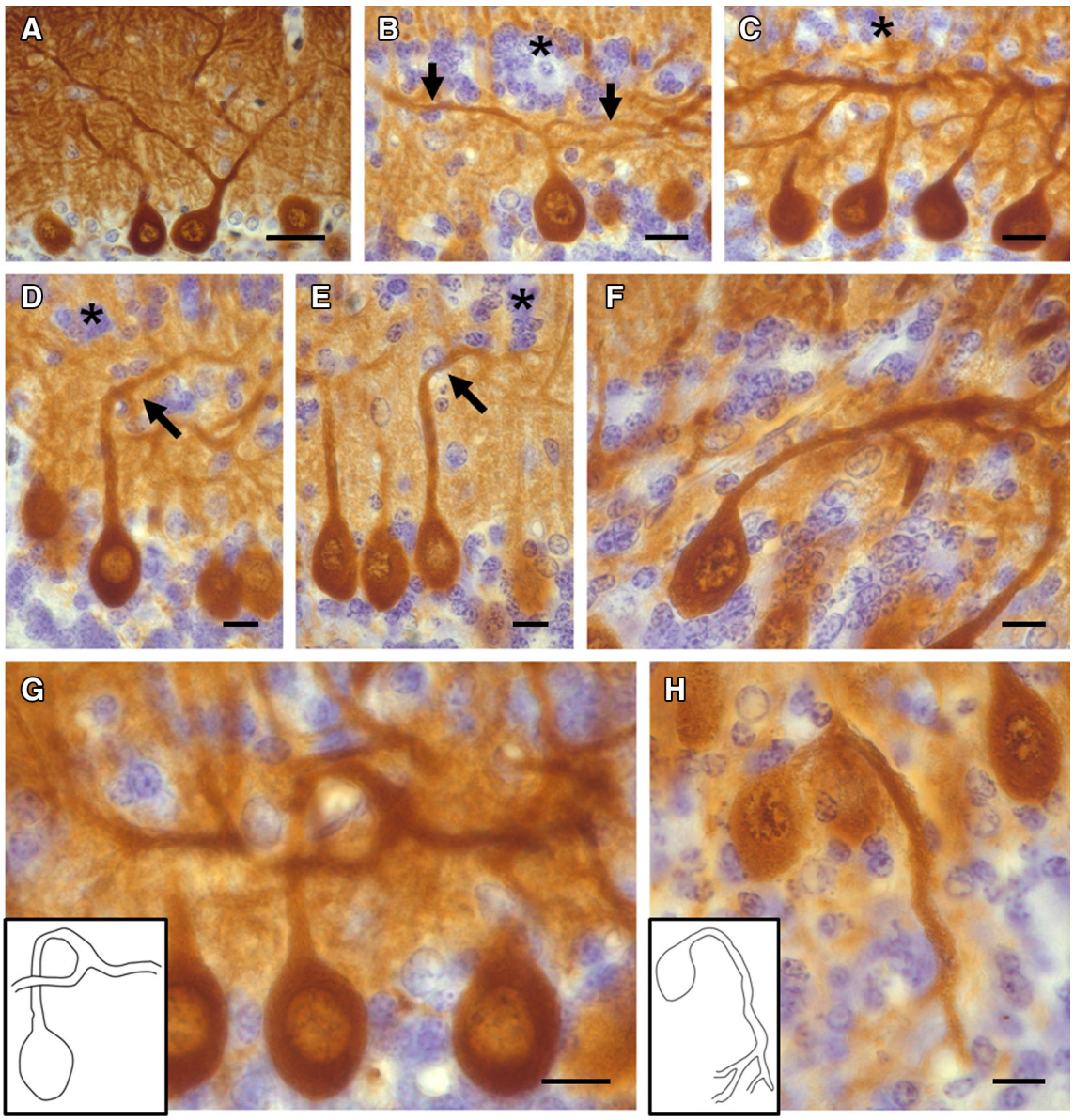

Fig. 7 Calbindin-immunostained Purkinje cells in saline-injected rats with ascending primary dendrites that repeatedly branch throughout the molecular layer (**a**) and HU-treated cerebella showing morphological alterations in the dendrite tree (**b**–**h**). *Asterisks* denote ectopic granule cells, and *arrows* indicate the altered dendritic tree. *Scale bar* 30 µm (**a**), 10 µm (**b**–**h**)

of neuron ectopia in each of the cerebellar cortex lobules are listed in Table 3.

Our observations also revealed that the dendritic alterations of PCs after HU treatment appear to occur in parallel with the depletion of GCs and the ectopia of these microneurons (Fig. 9).

Discussion

Sickle-cell anemia is an inherited hemoglobin disorder affecting millions of people throughout the world (McGann and Ware 2015). Estimates suggest that 250,000 children are born annually with this hematological disorder worldwide (Lervolino et al. 2011). HU has proven beneficial in the treatment of sickle-cell anemia (Rees 2015). Several studies have indicated that HU is a relatively safe drug in very young pediatric patients (McGann et al. 2012; Thornburg et al. 2012). Despite this, anemia and central nervous system abnormalities (ischemic lesions and stenoses) have been reported (Hankins et al. 2005).

In an attempt to evaluate the effects of HU exposure more rigorously, we supplied this cytotoxic agent to rats, in early postnatal life, and collected these at ages ranging from 6 h to 45 days. Our data indicate that a single administration of this agent induces substantial depletion of

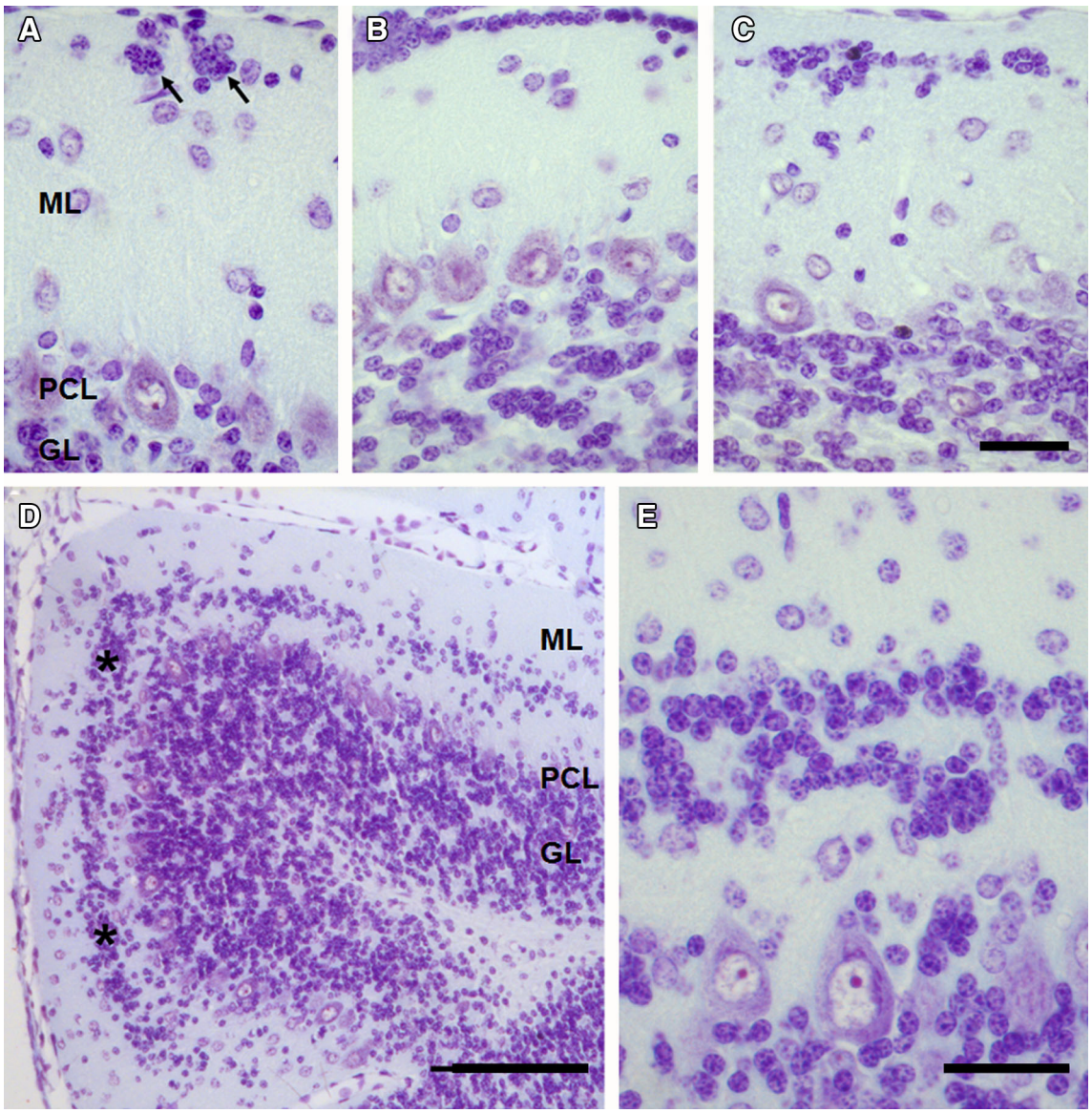

Fig. 8 Different patterns of granule cell ectopia in the cerebellar cortex of rats exposed to hydroxyurea. *ML* molecular layer, *PCL* Purkinje cell layer, *GL* granular layer. *Scale bar* in **a**–**c**, **e** 30 μm. *Scale bar* in **d** 100 μm

EGL cells, indicating that the cellular progenitors of GCs are highly vulnerable to early postnatal HU exposure. We show that P9 is a time of high susceptibility to environmental insults. In our experimental model, the EGL is able to resume proliferative activity after HU administration. A few cells escape the effect of the treatment with HU and reconstitute a new layer. This assumption is based on the fact that mitotic figures and BrdU-immunoreactive cells were found 21 h after HU treatment.

To study the effect of HU treatment on Bergmann glial, we determine the density of vimentin-stained cells. The quantitative analysis revealed a significant decreased in the density of this astroglial cell type in rats administered with HU at P9 with respect to control. This injection time is close to that reported, in which the proliferation of Bergman glia in the normal rat cerebellum reaches its peaks (Shiga et al. 1983; Finckbone et al. 2009). In saline rats, vimentin immunocytochemistry on sagittal sections of the cerebellar cortex revealed a typical palisade organization of vimentin-reactive Bergmann fibers ascending throughout the molecular layer. These results agree with other findings in terms of the pattern of staining of maturating Bergmann glia with antibody to vimentin (Lafarga et al. 1998). After a developmental injury induced by HU exposure, our results show overexpression of the cytoskeletal protein vimentin and thicker immunoreactive glial processes in those surviving Bergman glial cells. Disturbance of Bergmann glia processes was observed after a single injection of the

Table 3 Spatial disposition of ectopic GCs in the molecular layer

Area	Position of ectopic cells			
	Pattern 1	Pattern 2	Pattern 3	Pattern 4
Lobule I	+	–	–	–
Lobule II	–	+	–	–
Lobule III	–	+	–	–
Lobule IV	–	–	+	–
Lobule V	–	–	+	–
Lobule VIa	–	–	–	+
Lobule VIb	–	–	–	+
Lobule VII	–	–	–	+
Lobule VIII	–	–	–	+
Lobule IX	–	–	+	–
Lobule X	+	–	–	–
F. Prima	+	–	–	–
F. Secunda	+	–	–	–

Pattern 1 refers to the presence of small clusters of granule cells near the cerebellar surface. Pattern 2 corresponds to GCs aligned in a monolayer just beneath the pia mater. Pattern 3 indicates GCs imprecisely aggregated in a thin strip that is oriented parallel to the pial surface, and pattern 4 refers to GCs forming a wide and continuous band that lays parallel to the pia mater. F: fissure. The symbol "+" denotes the occurrence of a pattern in a given area of the cerebellar cortex

cytotoxic agents methylazoxymethanol (Lafarga et al. 1998) and cisplatin (Pisu et al. 2005), which produce depletion of the EGL cells and overexpression of GFAP in the distal portion of Bergmann fibers, including the end-feet at the pial surface. The last finding has been interpreted as a reactive response, in which changes in the interactions between Bergmann glia and GCs precursors have a role (Lafarga et al. 1998).

At P9, the EGL presents an organizational pattern consisting of a superficial stratum (proliferative layer), containing the bulk of proliferating cells and the inner premigratory layer presenting young GCs (Altman and Bayer 1997). The question arises whether the cells of both populations were affected or whether only the proliferating cells were damaged. The proposed mechanism of action by the cytotoxic agent HU is to decrease the production of deoxyribonucleotides necessary for DNA replication. This occurs via inhibition of the class I form of ribonucleotide reductase by inactivating the tyrosyl radical required for enzyme activity (Shao et al. 2006; Saban and Bujak 2009). The effect of the HU is cell cycle-specific; the drug is active in the S phase, producing an arrest of proliferating cell populations in the G_1/S phase of the cell cycle (Navarra and Preziosi 1999; Newton 2007). From these data, it appears that HU only affects proliferating cells in the EGL.

In the normal developing cerebellum, apoptotic nuclei occur naturally within the EGL (Lossi and Gambino 2008). Our findings indicate the density of apoptotic cells in the EGL of saline rats was very low at P9, which is in line with previous reports (Pisu et al. 2005). The balance of proliferating and apoptotic cells, and also premigratory cells, determines the thickness of the EGL, which represents an important factor in the cerebellum morphogenesis, since the variation of the EGL cells influences the density of GCs in the internal granular layer (Pisu et al. 2005; Cerri et al. 2011).

Present findings indicated that a severe depletion of EGL cells occurs as a consequence of HU treatment. Our results also indicate that the loss of these cellular precursors was due to apoptosis as evidenced by both the TUNEL procedure, which labels in situ fragmented DNA, and at the electron microscope level. Our ultrastructural study shows images of apoptosis such as chromatin condensation, nuclear fragmentation and presence of apoptotic bodies. In addition, it is worth indicating, in the present research, that we have found apoptotic events are not present differently in the superficial (convex) areas or along the fissures of a given cerebellar folium after treatment with HU, but that they occurred in the entire proliferative layer of the EGL. Activation of apoptosis has also been reported in the EGL within the first postnatal weeks in the homozygous *weaver* mice (Migheli et al. 1997) as well as after treatment with methylazoxymethanol (Lafarga et al. 1997), ethanol (Luo 2012) and cisplatin (Pisu et al. 2005).

We show that a single injection of HU in 9-day-old rats leads to a decrease in the vermal cerebellar size of rats sacrificed at P45, which is probably due to the loss of GC precursors. The demise of these neuroblasts originates lack of GCs in the internal granular layer. Our data also reveal that the HU modifies the normal settled patterns of PCs and GCs, and alters the morphology of the PC dendritic tree. All these events lead to an altered cytoarchitecture of the cerebellar cortex. At the time of HU administration (P9), we observed that PCs were aligned in a monolayer. However, when rats were collected at P45, these macroneurons were scattered in several irregular rows. We are far from being able to provide a clear explanation to this secondary disorientation, but it is known, from previous studies, that a condition of the monolayer dispersion of PCs is the rapid expansion of the EGL and the acquisition of GCs (Altman and Bayer 1997). We propose that, when the EGL is affected by HU treatment, this expansion does not take place. This may account for the failure in the dispersion of PCs. Moreover, our current data also suggested that the expansion of the cortical surface previous to HU injection does not seem to be sufficient for the accommodation of PCs. Our results corroborate the idea that the monocellular alignment of PCs is dependent on the production of an adequate number of GCs.

On the other hand, many GCs were arrested in the ML where they formed an ectopic zone. Several patterns of

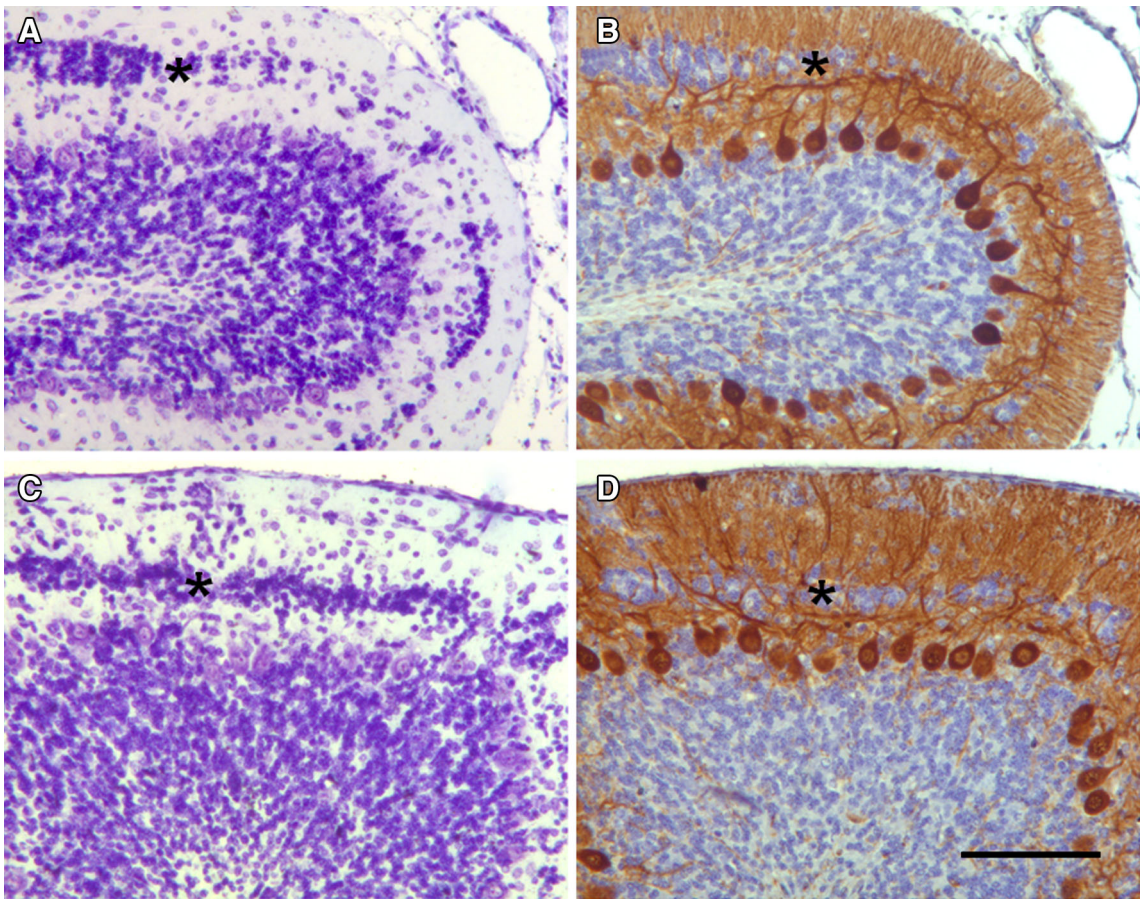

Fig. 9 Cerebellar sections from hydroxyurea-treated rats. **a**, **c** Paraffin sections stained with cresyl violet illustrating the presence of ectopic granule cell bands (*asterisks*) in the molecular layer. **b**, **d** Immunohistochemistry for Calbindin on consecutive sections, counterstained with haematoxylin. Most of these dendritic trees exhibit an abnormal orientation. Note also that these morphological changes occur simultaneously in regions where ectopic granule cell bands are present. *Scale bar* 100 μm

settlement were observed. We propose that the differences in the spatial distribution of ectopic neurons could be related to differences in the GC generation at the moment of HU exposure. Thus, in those regions presenting early- or mid-produced GCs, such as the superficial (convex) areas of the lobules I–V, IX, and the deep prima and secunda fissures (Altman and Bayer 1997), these microneurons were ectopically found near the cerebellar surface. However, in areas containing the late-generated granule cells—convex areas of the lobules VIa to VIII (Altman and Bayer 1997)—malpositioned neurons were observed forming a wide band placed in the middle of the ML and parallel to the pial surface.

Alterations of Bergmann glial cells can affect GC migration as seen in methylazoxymethanol (Lafarga et al. 1998), cisplatin (Pisu et al. 2005), or in neonatal X-irradiated rats (Li et al. 2006), resulting in an ectopic location of these neurons in the ML. Because Bergmann glial cells are the substrate for migration of young GCs (Komuro and Rakic 1998), our findings indicate that inward migration of young GCs from the EGL to the internal granule layer was affected. We suggest that the relationship between GCs and Bergmann glial processes may be altered due to HU exposition, resulting in an inappropriate neuron location. Moreover, the implication of mossy fibers in the immobilization of GCs should be also taken into account. This is because it has been reported that, in normal rats, the growth of the mossy fibers is synchronized with the descent of GCs and that both meet in the internal granular layer and form glomerular synapses (Altman and Bayer 1997). We propose that if the migration of differentiating and migrating GCs is temporally delayed, as by HU treatment, the ascending mossy fibers may continue their growth past the Purkinje cell layer and form synapses with these microneurons in the ML, which contribute to their immobilization.

In our model of injury, the altered migration of GCs and their location in the ML have important consequences on the normal development of the cerebellar cortex cytoarchitecture. The action of the HU appears to disorganize postnatal cerebellar development. That conclusion is based on two observations. First, PCs were scattered in several irregular rows, and their dendritic arbor morphology were

altered. Second, some GCs were ectopically located in the ML, suggesting that the migration of these microneurons was delayed.

The morphological changes observed in the PC dendritic arbor occur simultaneously in regions where ectopic GCs are present. The altered development of PC dendrites after HU treatment is likely due to changed guiding influence of parallel fibers. This event has been described in the morphological alterations induced by X-ray during postnatal development of the cerebellum (Altman and Bayer 1997), and in the *weaver* (Rakic and Sidman 1973; Sotelo 1975) and *reeler* mice (Mariani et al. 1977). Our results emphasize the idea that the generation and subsequent migration of GCs play important roles in the development of PC dendritic tree during the rats' postnatal life.

Conclusions

Despite several case reports indicating that HU is well-tolerated in pediatric patients (aged 6–24 months) and presents minimal secondary effects (Wang et al. 2001; Hankins et al. 2005), the results of the current study have important implications for the administration of HU to infants as the effects of this agent on the cerebellum might persist throughout their lives. Our study provides a clue for investigating the mechanisms of HU-induced toxicity in the postnatal development of the central nervous system. We show that a single injection of HU (2 mg/g) in 9-day-old rats leads to the activation of apoptotic cellular events, resulting in a substantial number of dying EGL cells and reactive response of the Bergmann glial cells. Our results also indicate that HU exposure decreases the vermal cerebellar size and produces dendritic alterations of Purkinje cells, which appear to occur in parallel with the loss of GCs and the ectopia of these neurons. The changes in the growth and remodeling of PCs are a proof of cerebellar plasticity. Further studies with laboratory animals receiving HU during the early postnatal life are required before this compound can be promoted as safe for infants.

Compliance with Ethical Standards

Conflict of interest The authors declare that they have no conflict of interest.

References

Altman J, Bayer SA (1997) Development of the cerebellar system: in relation to its evolution, structure and functions. CRC Press, Boca Raton

Bauer-Moffett C, Altman J (1977) The effect of ethanol chronically administered to preweanling rats on cerebellar development: a morphological study. Brain Res 119:249–268

Bernocchi G, Bottone MG, Piccolini VM, Dal Bo V, Santin G, De Pascali SA, Migoni D, Fanizzi FP (2011) Developing central nervous system and vulnerability to platinum compounds. Chemother Res Pract 2011:315418. doi:10.1155/2011/315418

Butts T, Green MJ, Wingate RJ (2014) Development of the cerebellum: simple steps to make a "little brain". Development 141:4031–4041

Cabrera O, Dougherty J, Singh S, Swiney BS, Farber NB, Noguchi KK (2014) Lithium protects against glucocorticoid induced neural progenitor cell apoptosis in the developing cerebellum. Brain Res 1545:54–63

Carletti B, Rossi F (2008) Neurogenesis in the cerebellum. Neuroscientist 14:91–100

Cerminara NL, Lang EJ, Sillitoe RV, Apps R (2015) Redefining the cerebellar cortex as an assembly of non-uniform Purkinje cell microcircuits. Nat Rev Neurosci 16:79–93

Cerri S, Piccolini VM, Santin G, Bottone MG, De Pascali SA, Migoni D, Iadarola P, Fanizzi FP, Bernocchi G (2011) The developmental neurotoxicity study of platinum compounds. Effects of cisplatin versus a novel Pt(II) complex on rat cerebellum. Neurotoxicol Teratol 33:273–281

Chedotal A (2010) Should I stay or should I go? Becoming a granule cell. Trends Neurosci 33:163–172

Contestabile A (2002) Cerebellar granule cells as a model to study mechanisms of neuronal apoptosis or survival in vivo and in vitro. Cerebellum 1:41–55

Dastjerdi FV, Consalez GG, Hawkes R (2012) Pattern formation during development of the embryonic cerebellum. Front Neuroanat. doi:10.3389/fnana.2012.00010

Dikranian K, Ishimaru MJ, Tenkova T, Labruyere J, Qin YQ, Ikonomidou C, Olney JW (2001) Apoptosis in the in vivo mammalian forebrain. Neurobiol Dis 8:359–379

Ebels EJ, Peters I, Thijs A (1975) Studies on ectopic granule cells in the cerebellar cortex. III. An investigation into the restoration of the external granular layer after partial destruction. Acta Neuropathol 31:103–107

Elmore S (2007) Apoptosis: a review of programmed cell death. Toxicol Pathol 35:495–516

Finckbone V, Oomman SK, Strahlendorf HK, Strahl C (2009) Regional differences in the temporal expression of non-apoptotic caspase-3-positive bergmann glial cells in the developing cerebellum. Front Neuroanat. doi:10.3389/neuro.05.003.2009

Hankins JS, Ware RE, Rogers ZR, Wynn LW, Lane PA, Scott JP, Wang WC (2005) Long-term hydroxyurea therapy for infants with sickle cell anemia: the HUSOFT extension study. Blood 106:2269–2275

Hervás JP, Martí-Clúa J, Muñoz-García A, Santa-Cruz MC (2002) Proliferative activity in the cerebellar external granular layer evaluated by bromodeoxyuridine labeling. Biotech Histochem 77:27–35

Jacobs B, Johnson NL, Wahl D, Schall M, Maseko BC, Lewandowski A, Raqhanti MA, Wicinski B, Butti C, Hopins WD, Bertelsen MF, Walsh T, Roberts JR, Reep RL, Hof PR, Sherwood CC, Manger PR (2014) Comparative neuronal morphology of the cerebellar cortex in afrotherians, carnivores, cetartiodactyls, and primates. Front Neuroanat. doi:10.3389/fnana.2014.00024

Jankowski J, Miething A, Schilling K, Baader SL (2009) Physiological Purkinje cell death is spatiotemporally organized in the developing mouse cerebellum. Cerebellum 8:277–290

Komuro H, Rakic P (1998) Distinct modes of neuronal migration in different domains of developing cerebellar cortex. J Neurosci 18:1478–1490

Komuro H, Yacubova E, Yacubova E, Rakic P (2001) Mode and tempo of tangencial cell migration in the cerebellar external granular layer. J Neurosci 21:527–540

Koppel H, Lewis PD, Padel AJ (1983) Cell death in the external granular layer of normal and undernourished rats: futher observations, including estimates of rate of cell loss. Cell Tissue Kinet 16:99–106

Lafarga M, Lerga A, Andres MA, Polanco JL, Calle E, Berciano MT (1997) Apoptosis induced by methylazoxymethanol in developing rat cerebellum: organization of the cell nucleus and its relationship to DNA and rRNA degradation. Cell Tissue Res 289:25–38

Lafarga M, Andres MA, Calle E, Berciano MT (1998) Reactive gliosis of immature Bergmann glia and microglial activation in response to cell death of granule cell precursors induced by methylazoxymethanol treatment in developing rat cerebellum. Anat Embryol 198:111–122

Lebwohl M, Menter A, Koo J, Feldman SR (2004) Combination therapy to treat moderate to severe psoriasis. J Am Acad Dermatol 50(3):416–430

Lervolino LG, Baldin PE, Picado SM, Calil KB, Viel AA, Campos LA (2011) Prevalence of sickle cell disease and sickle cell trait in national neonatal screening studies. Rev Bras Hematol Hemoter 33:49–54

Leto K, Rolando C, Rossi F (2012) The genesis of cerebellar GABAergic neurons: fate potential and specification mechanisms. Front Neuroanat. doi:10.3389/fnana.2012.00006

Li HP, Miki T, Yokoyama T, Lee KY, Gu H, Matsumoto Y, Wang ZY, Kawano H, Takeuchi Y (2006) Regional differences in vulnerability of the cerebellar foliations of rats exposed to neonatal X-irradiation. Neurosci Lett 402:86–91

Lossi L, Gambino G (2008) Apoptosis of the cerebellar neurons. Histol Histopathol 23:367–380

Lossi L, Merighi A (2003) In vivo cellular and molecular mechanisms of neuronal apoptosis in the mammalian CNS. Prog Neurobiol 69:287–312

Luo J (2012) Mechanisms of ethanol-induced death of cerebellar granule cells. Cerebellum 11:145–154

Manto M (2012) Toxic agents causing cerebellar ataxias. Handb Clin Neurol 103:201–213

Mariani J, Crepel F, Mikoshiba K, Changeux JP, Sotelo C (1977) Anatomical, physiological and biochemical studies of the cerebellum from reeler mutant mouse. Philos Trans R Soc Lond B 281:1–28

Martí J, Santa-Cruz MC, Bayer SA, Ghetti B, Hervás JP (2007) Purkinje cell age-distribution in fissures and in foliar crowns: a comparative study in the weaver cerebellum. Brain Struct Funct 212:347–357

Martí J, Santa-Cruz MC, Serra R, Molina O, Hervás JP, Villegas S (2013) Principal component and cluster analysis of morphological variables reveals multiple discrete sub-phenotypes in weaver mouse mutants. Cerebellum 12:406–417

Martí J, Santa-Cruz MC, Serra R, Hervás JP (2015) Systematic differences in time of cerebellar-neuron origin derived from bromodeoxyuridine immunoperoxidase staining protocols and tritiated thymidine autoradiographic: a comparative study. Int J Dev Neurosci 47:216–228

Martí J, Santa-Cruz MC, Serra R, Hervás JP (2016) Hydroxyurea treatment and development of the rat cerebellum: effects on the neurogenetic profiles and settled patterns of Purkinje cells and deep cerebellar nuclei neurons. Neurotox Res. doi:10.1007/s12640-016-9649-x

Martínez S, Andreu A, Mecklenburg N, Echevarria D (2013) Cellular and molecular basis of cerebellar development. Front Neuroanat. doi:10.3389/fnana.2013.00018

Marzban H, Del Bigio MR, Alizadeh J, Ghavami S, Zachariah RM, Rastegar M (2015) Cellular commitment in the developing cerebellum. Front Cell Neurosci 12(8):450. doi:10.3389/fncel.2014.00450

McGann PT, Ware RE (2015) Hydroxyurea therapy for sickle cell anemia. Expert Opin Drug Saf 14:1749–1758

McGann PT, Flanagan JM, Howard TA, Dertinger SD, He J, Kulharya AS, Thompson BW, Ware RE, for the BABY HUG investigators (2012) Genotoxicity associated with hydroxyurea exposure in infants with sickle cell anemia: results from the BABY-HUG phase III clinical trial. Pedriatr Blood Cancer 59:254–257

Migheli A, Piva R, Wei J, Attanasio A, Casolino S, Hodes ME, Dlouhy SR, Bayer SA, Ghetti B (1997) Diverse cell death pathways result from a single missense mutation in weaver mouse. Am J Pathol 151:1629–1638

Nakamura H, Sato T, Suzuki-Hirano A (2008) Isthmus organizer for mesencephalon and metencephalon. Dev Growth Differ 50(Suppl 1):S113–S118

Navarra P, Preziosi P (1999) Hydroxyurea: new insights on an old drug. Crit Rev Oncol Hematol 29:249–255

Newton HB (2007) Hydroxyurea chemotherapy in the treatment of meningiomas. Neurosurg Focus 23(4):E11

Oliveira SA, Chuffa LG, Fioruci-Fontanelli BA, Lizarte Neto FS, Novais PC, Tirapelli LF, Oishi JC, Takase LF, Stefanini MA, Martinez M, Martinez FE (2014) Apoptosis of Purkinje and granular cells of the cerebellum following chronic ethanol intake. Cerebellum 13:728–738

Paxinos G, Watson C (1998) The rat brain in stereotaxic coordinates, 4th edn. Academic Press, San Diego

Pisu MB, Roda E, Avella D, Bernocchi G (2004) Developmental plasticity of rat cerebellar cortex after cisplatin injury: inhibitory synapses and differentiating Purkinje neurons. Neuroscience 129:655–664

Pisu MB, Roda E, Guioli S, Avella D, Bottone MG, Bernocchi G (2005) Proliferation and migration of granule cells in the developing rat cerebellum: cisplatin effects. Anat Rec 287:1226–1235

Pu H, Wang X, Zhang J, Ma C, Su Y, Li X, Su L (2015) cerebellar neuronal apoptosis in heroin-addicted rats and its molecular mechanism. Int J Clin Exp Pathol 8:8260–8267

Rakic P, Sidman RL (1973) Sequence of development abnormalities leading to granule cell deficit in cerebellar cortex of weaver mutant mice. J Comp Neurol 152:103–132

Rees AL (2015) Hydroxyurea in pediatric patients with sickle cell disease: what nurses need to know. J Pedistr Oncol Nurs. doi:10.1177/1043454215614962

Saban N, Bujak M (2009) Hydroxyurea and hydroxamic acid derivatives as antitumor drugs. Cancer Chemother Pharmacol 64:213–221

Schlisser AE, Hales BF (2013) Deprenyl enhances the teratogenicity of hydroxyurea in organogenesis stage mouse embryos. Toxicol Sci 134:391–399

Shao J, Zhou B, Chu B, Yen Y (2006) Ribonucleotide reductase inhibitors and future drug design. Curr Cancer Drug Targets 6:409–431

Shiga T, Ichikawa M, Hirata Y (1983) Spatial and temporal pattern of postnatal proliferation of Bergmann glial cells in rat cerebellum: an autoradiographic study. Anat Embryol 167:203–211

Sillitoe RV, Joyner AL (2007) Morphology, molecular codes, and circuitry produce the three-dimensional complexity of the cerebellum. Annu Rev Cell Dev Biol 23:549–577

Smeyne RJ, Goldowitz D (1989) Development and death of external granular layer cells in the weaver mouse cerebellum: a quantitative study. J Neurosci 9:1608–1620

Sotelo C (1975) Anatomical physiological and biochemical studies of the cerebellum from mutant mice II. Morphological study of cerebellar cortical neurons and circuits in the weaver mouse. Brain Res 94:19–44

Sultan F, Glickstein M (2007) The cerebellum: comparative and animal studies. Cerebellum 6:168–176

Suzuki-Hirano A, Harada H, Sato T, Nakamura H (2010) Activation of Ras-ERK pathway by Fgf8 and its downregulation by Sprouty2 for the isthmus organizing activity. Dev Biol 337:284–293

Tanaka M (2015) The dendritic differentiation of Purkinje neurons: unsolved mystery in formation of unique dendrites. Cerebellum 14:227–230

Thornburg CD, Files BA, Luo Z, Miller ST, Kalpatthi R, Lyer R, Seaman P, Lebensburger J, Alvarez O, Thompson B, Ware RE, Wang WC, for the BABY HUG investigators (2012) Impact of hydroxyurea on clinical events in the BABY HUG trial. Blood 120:4304–4310

Wang WC, Wynn LW, Rogers ZR, Scott JP, Lane PA, Ware RE (2001) A two-year pilot trial of hydroxyurea in very young children with sickle-cell anemia. J Pediatr 139:790–796

Ware RE, Despotovic JM, Mortier NA, Flanagan JM, He J, Smeltzer MP, Kimble AC, Aygun B, Wu S, Howard T, Sparreboom A (2011) Pharmacokinetics, pharmacodynamics, and pharmacogenetics of hydroxyurea treatment for children with sickle cell anemia. Blood 118:4985–4991

Woo GH, Katayama K, Jung JY, Uetsuka K, Bak EJ, Nakayama H, Doi K (2003) Hydroxyurea (HU)-induced apoptosis in the mouse fetal tissues. Histol Histopathol 18:387–392

Woo GH, Katayama K, Bak EJ, Ueno H, Tamauchi H, Uetsuka K, Nakayama H, Doi K (2004) Effects of prenatal hydroxyurea-treatment on mouse offspring. Exp Toxicol Pathol 56(1–2):1–7

Woo GH, Bak EJ, Katayama K, Dai K (2006) Molecular mechanisms of hydroxyurea (HU)-induced apoptosis in the mouse fetal brain. Neurotocol Teratol 28:125–134

Wullimann MF, Mueller T, Distel M, Babaryka A, Grothe B, Köster RW (2011) The long adventurous journey of rhombic lip in jawed vertebrates: a comparative developmental analysis. Front Neuroanat 21(5):27. doi:10.3389/fnana.2011.00027

Xu H, Yang Y, Tang X, Zhao M, Liang F, Xu P, Hou B, Xing Y, Bao X, Fan X (2013) Bergman glia function in granule cell migration during cerebellum development. Mol Neurobiol 47:833–844

Zala C, Rouleau D, Montaner JS (2000) Role of hydroxyurea in treatment of disease due to human immunodeficiency virus infection. Clin Infect Dis 30:S143–S150